# Carboniferous–Permian interglacial warming and volcanism temporally linked to the world's oldest alkaline lake deposit of the Fengcheng Formation, NW China

**Deyu Gong[1*], Zeyang Liu[2*], Chuanmin Zhou[1], Emma Ownsworth[3], David Selby[3], Wenjun He[4], Zhijun Qin[4]**

[1]Research Institute of Petroleum Exploration & Development, PetroChina, Beijing 100083, China

[2]State Key Laboratory of Oil and Gas Reservoir Geology and Exploitation, Chengdu University of Technology, Chengdu, Sichuan 610059, China

[3]Department of Earth Sciences, University of Durham, Durham DH1 3LE, UK

[4]Xinjiang Oil Company, PetroChina, Xinjiang, Karamay 834000, China

[*]Corresponding author:

D.G. (deyugong@petrochina.com.cn); Z.L. (geozy.liu@outlook.com)

**Abstract**

In addition to being an important lacustrine hydrocarbon source rock, the Fengcheng Formation possesses well-preserved sodium-carbonate evaporite units and tuff beds. Known ancient alkaline salt-lake deposits bearing sodium-carbonate evaporite minerals like the Late Paleozoic Fengcheng Formation are limited beyond the modern day. However, hitherto the absolute age of the alkaline lacustrine Fengcheng Formation of the Junggar Basin (China) is debated (Late Carboniferous and/or Early Permian), and therefore its temporal link to a specific stage of the Late Paleozoic Ice Age (LPIA) remains unclear. Here, new Re–Os geochronology demonstrates that the Fengcheng Formation is predominately of Late Carboniferous-age (304.4 to 297.3 Ma), and therefore its deposition coincides with the interglacial climate warming interval between glaciation C4 and P1 of the LPIA and not the younger interglacial stages as previously proposed. The Re–Os isotope systematics indicate that the lake water column during the deposition of the Fengcheng Formation had a relatively unradiogenic Os ($^{187}Os/^{188}Os$, $Os_i$) isotope composition (0.32 to 0.36), which is in contrast to the typical radiogenic $Os_i$ recorded for lacustrine deposits throughout geological time. The unradiogenic $Os_i$ for the Fengcheng Formation ties the source of the Os in the lake to the weathering of adjacent mafic volcanic rocks and/or hydrothermal input (~0.13). As a result, the penecontemporaneous relationship to the Late Paleozoic interglacial climate warming (causing enhanced evaporation) coupled with weathering of volcanic rocks and/or hydrothermal fluid input into the lake is considered to have been

mechanistic in the formation of an alkaline salt lake dominated by sodium and carbonate.

**Keywords:** Re–Os, evaporite, lacustrine, volcanism, organic matter type

## 1. Introduction

Beyond the present-day alkaline lakes (e.g., Mono Lake and Walker Lake, USA; Chahan Lake, China; Turkana Lake and Magadi Lake, Kenya; Timms, 2022), and the Paleogene Hetaoyuan Formation (China, Yang et al., 2014) and Eocene Green River Formation (USA; Lowenstein et al., 2017; Cummings et al., 2012), the Late Paleozoic Fengcheng Formation of the Junggar Basin in northwestern China, represents one of the oldest known records of deposition in a saline lacustrine basin (Cao et al., 2020). The Fengcheng Formation has been assigned an Early Permian-age based on relative dating techniques such as biostratigraphy, lithostratigraphy, chemostratigraphy and structural relationships (Feng et al., 2018; Wang et al., 2022). The current absolute age control of the lacustrine Fengcheng Formation (U–Pb zircon detrital and interbedded tuff beds) exhibit considerable discrepancy (up to 25 Myrs; Wang et al., 2021; 2022). Thus, any relationship to global/regional tectonic and deposition processes, in addition to stratigraphic correlation is hitherto poorly constrained and debated. To date, the depositional timing of the Fengcheng Formation is considered to broadly overlap with the stages of the Late Paleozoic Ice Age (LPIA) – an extended ice house event that spanned ~70 Myrs (Montañez and Poulsen, 2013) and is recorded by eight glacial and nonglacial intervals (Fielding et al., 2023). Thus, the absolute age of the Fengcheng Formation is key to directly link its formation with a specific glacial stage of the LPIA. Moreover, interbedded tuffaceous sandstone, andesite and basalt of Fengcheng Formation basal Member 1 suggests an association with active magmatism during deposition that ultimately could have controlled the alkalinity of the lake and hence the formation of the sodium-carbonate-evaporite beds (Tosca and Tutolo, 2023).

Here we apply Re–Os geochronology to directly date the three members of the Fengcheng Formation to temporally correlate its deposition to the specific interglacial period of the LPIA (Fielding et al., 2023). Further, we utilise the initial Os isotope compositions derived from the Re-Os geochronology, together with petrographic investigations to discuss the role of volcanism with the formation of the saline lacustrine basin and the associated sodium-carbonate evaporite beds of the Fengcheng Formation.

## 2. Geological background

The Junggar Basin, located in the northern part of Xinjiang Uygur Autonomous Region, northwest China (Fig. 1), is a superimposed basin developed on a basement of crystalline Precambrian and Carboniferous aged sedimentary strata (Cao et al., 2020). The Mahu Sag is a secondary structural unit of the Central Depression located in the northwest sector of the Junggar Basin (Fig. 1). Following the juxtaposition of the Central Asian Orogenic Belt with the Junggar Basin during the Late Carboniferous, the basin experienced multiple intraplate tectonic events (e.g., Carroll et al., 1995; Tang et al., 2015; Yang et al., 2015). As a result, the Mahu Sag evolved from a syn-rift basin during the Early Permian to a post-rift basin in the Middle Permian, ending with a tectonic inversion between the Late Permian and Early Triassic (Tang et al., 2021; Yang et al., 2023). The Lower (Jiamuhe and Fengcheng formations) and Middle (Xiazijie and

Lower Wuerhe formations) Permian strata were deposited during the syn-rift to post-rift stages, respectively.

The Fengcheng Formation was primarily deposited in a fan-delta-lacustrine environment under seasonally alternating humid and arid conditions that was associated with high salinity. The formation is subdivided into three members. The basal Member 1 unconformably overlies the Jiamuhe Formation that consists primarily of volcanic rocks. Member 1 is composed of volcanic rocks in its lower part and dolomitic mudstone interbedded with siltstone in its upper part. Member 2 has limited exogenous input and was deposited in a highly saline environment. It is characterized by thick organic-rich dolomitic rocks and mudstones with widely developed sodium-carbonate (e.g., wegscheiderite, trona, nahcolite) beds ranging from mm– to dm–scale. Member 3 is characterized by lithologies similar to the top part of Member 1, but also records a decrease in salinity and an increase in exogenous input (e.g., Wang et al., 2021). An upper Early Permian age, based on biostratigraphy, lithostratigraphy, and structural relationships, has been assigned to the Fengcheng Formation (e.g., Feng et al., 2018). A maximum depositional age of the Fengcheng Formation of late to middle Early Permian is also proposed by detrital LA–ICP–MS zircon U–Pb dates (Lu, 2018; Tang et al., 2022; Gao et al., 2020). Yet, in stark contrast, zircons from interbedded tuff beds within Member 1 and 3 yielded LA–ICP–MS U–Pb dates up to 25 Myrs older (Wang et al., 2022).

## 3. Sample selection and methodology

Samples from the Fengcheng Formation were collected from the Maye 1 core in the Mahu Sag, Junggar Basin (Fig. 1; coordinates not available due to restrictions). Whole core programmed pyrolysis data of the entire core were used to target intervals for Re-Os geochronology. Specifically areas of high TOC (thus potentially enriched in Re and Os), and variable HI values (thus potentially possessing variable organic matter type that could yield variable $^{187}Re/^{188}Os$ ratios; Cumming et al., 2012; Liu et al., 2020a; Pietras et al., 2022). Eight samples over an interval of 2–4 m were collected from each of the three members (Fig. 2). Samples were firstly polished on a silicon carbide plate to remove any surface and metal contact from the drilling process. Samples were then broken into chips and crushed to a powder with an agate mill and puck in a shatterbox.

### *3.1 Organic petrology and geochemistry*

Ten samples were analysed for organic petrology. Optical microscopy analyses were conducted on thin rock sections. Samples were sectioned perpendicular to the bedding before being embedded in a homogeneous mixture of Buehler's epoxy resin and hardener (ratio 5:1). The latter were then dried and polished (Taylor et al., 1998; Amijaya and Littke, 2006). The thin rock sections were examined at different magnifications and under different light conditions (incident white light and blue light excitation) to characterize the organic matter using a Nikon LV 100 microscope. The vitrinite reflectance was measured using a Zeiss Scope A1 incident light microscope at a wavelength (λ) of 546 nm. The reflectance of samples rich in vitrinite particles was measured from at least 50 points. Samples were point-counted (300–500 points per sample) to determine relative abundances of mineral matter and macerals.

Twenty-four samples were analysed for total organic carbon (TOC) content using a LECO carbon analyser. On the same sample set to determine Tmax, oxygen and hydrogen index values, programmed pyrolysis was performed using a Rock-Eval 6 instrument.

### *3.2 Evaporite SEM evaluation*

The chemical composition of the evaporite minerals was determined from a fresh surface (coated with gold) using a scanning electron microscope, a TESCAN VEGA/XMU SEM, fitted with a BRUKER Quantax xFlash 6/30 energy-dispersive X-ray spectroscopy detector. X-ray powder diffraction (XRD) patterns of the evaporite minerals were obtained on a Rigaku D/Max 2500 VB2+/PC diffractometer with Cu Kα radiation. The extracted data were analyzed using Jade software (Version 6.5).

### *3.3 Re-Os geochemistry*

The rhenium–osmium (Re–Os) isotope analysis was carried out at the Durham Geochemistry Centre (Laboratory for Sulfide and Source Rock Geochronology and Geochemistry, and Arthur Holmes Laboratory) at Durham University. The analytical protocol uses the $Cr^{VI}$–$H_2SO_4$ digestion methodology to preferentially liberate hydrogenous Re and Os, and to limit incorporation of any detrital Re and Os (Selby and Creaser, 2003). About 1 g of sample powder with a known amount of mixed $^{190}Os$ and

$^{185}Re$ tracer (spike) solution and 8 ml of 0.25 g/g $Cr^{VI}$–$H_2SO_4$ solution were placed and sealed into a carius tube and heated at 220°C for 48 h. Osmium was purified by solvent extraction ($CHCl_3$) and micro-distillation methods (Birck et al., 1997; Cohen and Waters, 1996). Rhenium was separated and purified from the Os-extracted $Cr^{VI}$–$H_2SO_4$ solution using NaOH–$C_3H_6O$ solvent extraction and anion chromatography. The purified Re and Os fractions were loaded onto Ni and Pt filaments, respectively (Selby et al., 2007). Isotopic measurements were determined using a ThermoScientific TRITON mass spectrometer using static Faraday collection for Re and secondary electron multiplier in peak-hopping mode for Os. Total procedural blanks during this study were 15.6 ± 0.45 pg and 0.035 ± 0.007 pg (1σ S.D., n = 3) for Re and Os, respectively, with an average $^{187}Os/^{188}Os$ value of 0.18 ± 0.01.

The initial $^{187}Os/^{188}Os$ composition ($Os_i$) were calculated from the Re-Os isotope compositions using the $^{187}Re$ decay constant $1.666\times10^{-11}$ $yr^{-1}$ (Smoliar et al., 1996) and the ages derived from the isochron. Repeat analyses of reference material SDO-1 and SBC-1suggest ≤ 0.05 variation in calculated $Os_i$ (Du Vivier et al., 2014; 2015; Sproson et al., 2022).

## 4. Results

### *4.1 Organic petrology and geochemistry*

The Fengcheng Formation Member 1 possesses lower TOC values (0.42 to 0.60 %, average 0.50 %) than Member 2 (0.55–2.00 %, average 1.03 %) and Member 3 (0.40–2.14 %, average 1.05 %). All samples are characterised by a Type II–III kerogen based on Hydrogen–Oxygen Index plots (Fig. 3), with exceptionally good hydrocarbon potential. All samples exhibit a moderate thermal maturity (Tmax = 407 – 442 °C, Ro = 1.05 – 1.30 %). Organic petrology reveals large variations in exinite, vitrinite and inertinite contributions among the samples (Fig. 4). The samples have exinite amounts ranging from 0 to 67.7 %, vitrinite ranging from 14.7 to 62.5 %, and inertinite from 9.1 to 53.3 %, respectively (Table S2). Members 1 and 3 have moderate to high exinite content. In contrast, samples from Member 2 have no exinite. Member 2 has higher vitrinite contents (29.6 – 62.5%) compared with the other two members (14.7 – 35.7%).

### *4.2 Evaporite mineral SEM observation*

An x-ray diffractogram is used to determine the mineral composition of the bedded evaporite minerals in the Fengcheng Formation. The analysis shows the presence of wegscheuderite, trona, natron, pirssonite, nahcolite, and reedmergnerite (Fig. 5b). A thin evaporite bed observed in a core sample is primarily composed of trona needles (Fig. 5c). Columnar trona crystals interspersed with rhombic reedmergnerite crystals is observed under cross-polarized light (Fig. 5d). The back-scattered electron image of the evaporite reveals intercalated columnar trona crystals with pirssonite and reedmergnerite. The evaporite bed also displays ordered to sub-ordered halite (NaCl) crystals, prismatic nahcolite crystals, and disordered thenardite ($Na_2SO_4$) crystals. These crystals may have formed as secondary minerals during sample preparation, such as during ion milling. The energy dispersive X-ray spectroscopy analysis of natron and pirssonite shows the presence of a gold coating, as indicated by the element Au (Fig. 5e and 5f).

*4.3 Re–Os geochemistry*

Rhenium and osmium concentrations range from 5.2 – 19.5 ppb and 64.7 – 127.6 ppt for Member 1, 7.5 – 21.8 ppb and 77.2 – 156.8 ppt for Member 2, 11.9 – 37.4 ppb and 136.3 – 422.7 ppt for Member 3, respectively. These intervals are generally characterised by a large range in $^{187}Re/^{188}Os$ values (Member 1 = 433.0 to 1652.6, Member 2 = 404.0 to 1463.4, Member 3 = 558.5 to 866.7). Using the inverse isochron method in IsoplotR the Re-Os data yield Model 3 Re–Os dates of 304.4 ± 1.7 [2.5 including decay constant] Ma (n = 4, 2σ; MSWD = 2.9) for Member 1, 300.1 Ma ± 1.9 [2.6] Ma (n = 5, 2σ; MSWD = 4.7) for Member 2, and 297.3 Ma ± 4.7 [5.0] Ma (n = 6, 2σ; MSWD = 4.8) for Member 3 (Li and Vermeesch, 2021; Vermeesch, 2018). Initial Os isotope compositions are 0.33 ± 0.02 for Member 1, 0.36 ± 0.02 for Member 2 and 0.32 ± 0.05 for Member 3, respectively. The uncertainty in the Re–Os dates can be accounted for by the possible duration sampled for each member and the variation in the initial $^{187}Os/^{188}Os$ (Member 1 = 0.024, Member 2 = 0.039, Member 3 = 0.026).

Monte Carlo simulations (Li et al., 2019) yielded identical results to those of the inverse isochron method (Fig. 2). The Monte Carlo simulations suggest that analytical uncertainties account for 30-61% of the total uncertainties of the final ages (Fig. 2). The rest of the date uncertainty is a function of the model age uncertainties.

## 5. Discussion

### *5.1 Age reassignment for the Fengcheng Formation*

Relative dating techniques (biostratigraphy, lithostratigraphy, chemostratigraphy and structural relationships) have been used to suggest an Early Permian age for the Fengcheng Formation (Feng et al., 2018; Wang et al., 2022). Detrital LA-ICP-MS zircon U–Pb dates from Members 1 and 3 of the Fengcheng Formation from cores FN-4, JL-17 and DT-1, ~75 kms from the Maye 1 core (Fig. 1) have been used to propose that the maximum depositional age of the Fengcheng Formation is middle to late Early Permian ranging between 284 ± 4 (Member 1 – FN-4) to 278.9 ± 1.3 Ma (Member 1 – JL-17); 277.4 ± 2.8 Ma (Member 3 – DT-1) (2σ; Lu, 2018; Tang et al., 2022; Fig. 2), which would suggest that the Fengcheng Formation was deposited during the interglacial interval associated with warm and arid climate conditions across the mid-latitude of the northern hemisphere between glaciation P2 and P3 (Fielding et al., 2023; Montañez and Poulsen, 2013).

In contrast to detrital zircon U–Pb dates, magmatic zircons from volcanic tuff beds within the Fengcheng Formation of X76, X88, X201 cores ~30 km from the Maye 1 core yielded LA-ICP-MS $^{206}Pb/^{238}U$ dates up to 25 Myrs older (Wang et al., 2021; 2022). Zircons from a tuff in Member 3, 27 m above the Member 2-3 boundary yielded a date 296.8 ± 2.5 Ma (2σ; MSWD = 2 – unknown if the decay constant uncertainty is included, although its affect is only ~20 - 40 Kyrs). Five LA-ICP-MS $^{206}Pb/^{238}U$ dates have been obtained from interbedded tuff beds within Member 1 (including three from cores X76, one from, X88 and one from X201). There is broad agreement between three of the LA-ICP-MS $^{206}Pb/^{238}U$ dates (X76-3646.06 = 300.16 ± 0.61 Ma; X76-3646.50 = 300.7 ± 1.3 Ma; X201-4923.70 = 300.8 ± 1.3 Ma), however, another two LA-ICP-MS $^{206}Pb/^{238}U$ dates are older (X76-3645.60 = 304.94 ± 0.68 Ma; X88-3827.50 = 305.1 ± 1.2 Ma) and do not uphold the law of superposition (Wang et al., 2021; 2022). Although, a weighted LA-ICP-MS $^{206}Pb/^{238}U$ date of 302.34 ± 0.73 Ma (MSWD = 2.0; N = 122) for Member 1 has been presented, given that the dated tuff beds are below the Kasimovian–Gzhelian Boundary Interval $\delta^{13}C$ negative excursion (ca. 304 Ma) the older LA-ICP-MS $^{206}Pb/^{238}U$ dates (ca. 305 Ma) are proposed to be a more accurate date of Member 1 (Wang et al., 2022).

Although the magmatic zircon U–Pb ages could be affected by a xenocrystic component, pre-eruptive closure of the zircon U–Pb systematics, Pb loss, and/or detrital grains (as discussed by Wang et al., 2022), in contrast Re–Os dates of organic-rich sedimentary rocks provide direct depositional age constraints. The Re–Os dates are nominally young from Member 1 (304.4 ± 1.7 [2.5] Ma) to 3 (297.3 ± 4.7 [5.0] Ma), although dates from Members 2 (300.1 Ma ± 1.9 [2.6] Ma) and 3 (297.3 ± 4.7 [5.0] Ma), overlap when considering lower and upper age uncertainties (Figs. 2 and 6). Further there is nominal agreement of the Re-Os sedimentary rock and the LA-ICP-MS $^{206}Pb/^{238}U$ zircon dates (Fig. 6).

Eight distinct glacial and nonglacial periods have been identified in the Carboniferous and Permian systems of eastern Australia (Fielding et al., 2023). These glacial intervals are interspersed with intervals where evidence of glacial episodes are not preserved. The Carboniferous period has four relatively short-lived glacial intervals (C1–C4), which were followed by four longer-lived glaciations (P1–P4) during the Permian period. Between the Carboniferous and Permian glaciations, there was a significant nonglacial period during the Late Carboniferous. Given that the age of the Carboniferous–Permian boundary is defined to 298.9 ± 0.15 Ma (Schmitz, 2020), the Re-Os dates of this study imply that the majority of the Fengcheng Formation (specifically Members 1 and 2; Fig. 6) is uppermost Carboniferous in age and therefore penecontemporaneous with an interglacial period between glaciation C4 and P1 of LPIA (Wang et al., 2022; Fielding et al., 2023). The agreement of the U-Pb and Re-Os dates for Member 3 (296.8 ± 2.5 Ma; Wang et al., 2022; 297.3 ± 4.7 [5.0] Ma; this study, respectively), although they overlap within uncertainty with the age of the Carboniferous–Permian boundary (298.9 ± 0.15 Ma), does imply that Member 3 is earliest Permian in age. The new Re-Os ages yield a nominal rate of sedimentation estimate during the deposition the Fengcheng Formation of 13 to 72 m/Myr.

*5.2 Initial Os isotope compositions record volcanic input into the Junggar basin*

Lacustrine sediments of the geological record are generally characterised by radiogenic $Os_i$ values, as most of the Os is derived from riverine input through continental weathering, due to the elevated Re/Os ratios compared with mantle materials (average continental mass $^{187}Os/^{188}Os$ = ~1.4; Peucker-Ehrenbrink and Ravizza, 2000). For example, lacustrine units of the Toarcian (Jurassic) Da’anzhai Formation of the Sichuan

Basin (China) have $Os_i$ values of ~1.3 (Xu et al., 2017), which are much higher than the Early Jurassic open marine $Os_i$ values of 0.4 – 0.8 recorded from Europe (Kemp et al., 2020; Percival et al., 2016; Them et al., 2017). The Eocene Green River Formation has $Os_i$ values of 1.4 – 1.5 (Cumming et al., 2012; Pietras et al., 2020) that are also much higher than the coeval open marine Os isotope value of ~0.6 (Kato et al., 2011). Likewise, radiogenic $^{187}Os/^{188}Os$ (up to 1.3 at ~36 Ma) compositions are reported for the Arctic Ocean's 'lake stage' prior to connection of the lake with the global ocean which is characterized by a decrease in the $Os_i$ to the ~36 Ma marine Os signature of ~0.6 (Poirier and Hillaire-Marcel, 2011). The increase in the $^{187}Os/^{188}Os$ (from 0.39 to 0.55) of Arctic Ocean seawater preceding the onset of the Paleocene–Eocene thermal maximum has been explained by a reduction in the flux of less radiogenic Os into the Arctic Basin due to hydrological restriction in the basin (Dickson et al., 2015). A highly radiogenic $Os_i$ of 1.97 has been reported for the Ipubi Formation black shales of the Araripe Basin, suggesting deposition in a highly restricted lacustrine setting (Lúcio et al., 2020).

In contrast, the $Os_i$ of the Fengcheng Formation is characterised by very low values of 0.32 – 0.36 (Fig. 2). An episodic connection with the open ocean has been proposed during the deposition of the Fengcheng Formation (Zhang et al., 2007). Marine incursion would encourage the exchange of local water mass with seawater that would drive the Os isotope values towards the marine Os isotope composition (Poirier and Hillaire-Marcel, 2011). Available data suggest that the Late Carboniferous ocean was characterised by an Os isotope composition of ~0.55 (Tripathy et al., 2015). A similar Os-isotope composition is reported for the Early and Late Permian ~0.6 (Liu and Selby, 2021). Although, the Late Permian Os-isotope record displays excursions to non-radiogenic values associated with the volcanism of the Siberian traps and/or South China (Liu and Selby, 2021; Liu et al., 2020b).

Assuming a gradual evolution of the marine $Os_i$ profile without any major perturbations, the marine $Os_i$ values for the Late Carboniferous and Early Permian likely fall between 0.55 and 0.61 (Fig. 7). Therefore, any marine incursion during the deposition of the Fengcheng Formation could only drive the Os-isotope composition of the water column towards a minimum value of 0.55, assuming total exchange between the lacustrine water mass with that of seawater, rather than the observed $Os_i$ compositions of 0.32 – 0.36 (Fig. 2). Moreover, any marine incursion during the deposition of the Fengcheng Formation is suggested to have been only episodic, and thus our samples could not have coincidentally included these incursions (Zhang et al., 2007). Furthermore, evidence from nitrogen isotopes, lithofacies, geochemistry of the associated sediments, and the presence of alkali minerals suggest a lacustrine alkaline depositional environment for the Fengcheng Formation (Cao et al., 2020). The latter may indicate a hydrologically closed basin (Lowenstein et al., 2017), with the water column dominated by $Na^+$, $HCO_3^-$ and $CO_3^{2-}$ ions (Boros and Kolpakova, 2018). Thus, we consider any marine incursion unlikely to have caused the unradiogenic $Os_i$ values of the Fengcheng Formation. An alternative and plausible explanation for the unradiogenic $Os_i$ is the input of unradiogenic Os from the weathering of volcanic juvenile mafic rocks within the hydrological catchment of the alkaline lake, which are common to the western Junggar region (e.g., Late Paleozoic [~347 – 287 Ma] granitoids and volcanic rocks; Tang et al., 2012).

*5.3 Implications for soda lake formation*

As the oldest known soda lake deposit (Cao et al., 2020), the Fengcheng Formation is dominated by dolomitic and limy shales, intercalated with cm– to dm–scale sodium-carbonate beds in Member 2 and the basal section of Member 3 near the centre of the Mahu Sag. The sodium-carbonate beds consist of several evaporite minerals (Fig. 4), such as wegscheiderite $Na_5H_3(CO_3)$, trona ($Na_2H(CO_3O_2 \cdot 2H_2O)$), natron, nahcolite ($NaHCO_3$), natrite ($Na_2CO_3$), northupite ($Na_3Mg(CO_3)_2Cl$) and pirssonite ($Na_2Ca_2(CO_3)_3$)， most of which have been previously identified (Cao et al., 2020). Interestingly, halite, which is common in the Green River Formation and indicates higher salinity, is rarely observed in the Fengcheng Formation (Fig. 4e). Most of the sodium-carbonate minerals of the Fengcheng Formation are typical of soda lake (or alkaline saline lake) deposits, such as the Green River Formation (Milton and Fahey, 1960) and the Searles Lake deposit (Eugester and Hardie, 1978). Soda lake deposits, which are unusual deposits that are almost entirely limited to the Cenozoic (Eocene, Miocene, Pleistocene, Holocene) (Earman et al., 2005; Warren, 2010), typically precipitate from brines with elevated $Na^+$ and $CO_3^{2-}{}_{TOT}$ ([$HCO_3^-$] + [$CO_3^{2-}$] + $H_2CO_3^*$], where bracketed symbols refer to concentration) relative to $Ca^{2+}$ and $Mg^{2+}$ (Earman et al., 2005). The rarity of the soda lake deposit of the Permian Fengcheng Formation makes it a valuable analogue for studying Cenozoic alkaline lake sediments.

5.3.1 Evaporative concentration of brines

The prevailing theory for the formation of trona deposits is the evaporative concentration of brines whereby $Na^+$ and $HCO_3^-$ + $CO_3^-$ ions dominate due to silicate hydrolysis of volcanic rocks or volcaniclastic sediments (Boros and Kolpakova, 2018; Earman et al., 2005; Jones et al., 1977). The climate associated with the deposition of massive carbonates of Member 2 of the Fengcheng Formation is consistent with its new temporal placement based on Re–Os ages to the Late Carboniferous interglacial between C4 and P1 of the LPIA (Fig. 2). During the warmer climate of the interglacial, intense evaporation will consequently lead to the precipitation of alkaline earth carbonates and sodium-carbonates that are common to the Fengcheng Formation. The warm climate may be linked to elevated atmosphere $CO_2$ levels associated with greenhouse gas emissions from volcanic degassing and/or sill bodies that intruded organic-rich units (Svensen et al., 2009) around the Central Asian Orogenic Belt (CAOB) (Şengör et al., 1993). The high atmospheric $CO_2$ levels may be indicated by appearance of nahcolite in Member 2 and 3 of the Fengcheng Formation based on experimental data (Jagniecki et al., 2015). The decrease of the evaporates in Member 3 might be linked to a shift to a cooler climate during the Early Permian during the onset of glacial episode P1 of the LPIA (Fielding et al., 2023).

The deposition of the Fengcheng Formation is accompanied by contemporaneous mafic volcanism which is indicated by the unradiogenic Os isotope compositions (Fig. 2), and intercalated basalt and tuff beds (Wang et al., 2022) in the Lower-Mid Fengcheng Formation. The sustained intense volcanism from the Late Carboniferous to the Early Permian in the Mahu Sag region (or CAOB) (Li et al., 2015) may have injected abundant volcanic $CO_2$ into the atmosphere and paleo-Mahu Lake. During the migration of $CO_2$-oversaturated hydrothermal fluids from active thrust faults which developed in the foreland of the West Junggar Orogenic Belt, the reaction of magmatic-derived $CO_2$(aq) with country rocks would result in the formation of waters with excess alkalinity and $Na^+$ (Earman et al., 2005; Lowenstein et al., 2017). The aerobic decay of organic matter may have also acted as an important source of $CO_2$ for the Fengcheng Formation because most of the sedimentary facies are grey massive mudstones indicating deposition in a stratified lake frequently interrupted by storm-floods (Gong et al., 2024). Microbial $CH_4$ production is suggested to have occurred in the paleo-Mahu lake, with an estimated ∼10 – 109 Gt of biogenic $CH_4$ suggested to have been emitted, which could have been converted to $CO_2$ (Xia et al., 2023). Although the existence of nahcolite may indicate an elevated $CO_2$ content of the gas phase (1475 to 20,300 ppm between 20-60 ºC; Eugster, 1966), it has been proposed that the $CO_2$ sourced from magmatism and aerobic organic decay are more common in the formation of sodium-carbonate in the Fengcheng Formation. Further, the impact of atmospheric $CO_2$ concentration is relatively minor to soils that typically have higher $p$$CO_2$ than the atmosphere (~400 ppm) (Eugester and Hardie, 1978), and moreover the average $pCO_2$ of surface water of saline lakes is 5–8 times higher than that of the atmosphere (Duarte et al., 2008).

### 5.3.2 Weathering of volcanic rocks

Weathering reactions of volcanic rocks or volcaniclastic sediments are suggested to typically produce waters that are initially dominated by $Na^{+}$ and $HCO_3^{2-}$ ions over $Ca^{2+}$ and $Mg^{2+}$ (Boros and Kolpakova, 2018; Earman et al., 2005), especially via the hydrolysis of sodium-rich minerals (e.g., albite). The West Junggar region has extensive subaerial and subsurface intermediate–acidic volcanic rocks (or volcaniclastics derived from them) of Carboniferous and Permian age (Li et al., 2015), which could have fed the paleo-Mahu Lake with waters dominated by $Na^{+}$, $HCO_3^{2-}$ and $Ca^{2+}$ ions. The average mole ratio of $Na^{+}/(Mg^{2+}+Ca^{2+})$ of basaltic andesite in the Fengcheng Formation is ~1 (Table 1), which is greater than the global average value (~0.7) for andesite (Taylor, 1968), and thus favours the formation of saline waters.

## 6. Conclusions

New Re–Os dates for the three members of the Fengcheng Formation are in agreement with zircon ages from volcanic tuffs. The new Re–Os ages place the majority of the Fengcheng Formation (Member 1 and 2) below the Carboniferous–Permian Boundary (298.9 ± 0.15 Ma). As such, most of the deposition of the Fengcheng Formation occurred during the interglacial period C4–P1 of the Late Paleozoic Ice Age that was associated with high $pCO_2$ atmospheric levels. The nonradiogenic initial Os isotope compositions of 0.32–0.36 of the Fengcheng Formation are distinct from the radiogenic initial Os isotope compositions that are typical to lacustrine units of the geological record. The nonradiogenic $Os_i$ compositions of the Fengcheng Formation are interpreted to be caused by the input of unradiogenic Os through the weathering of adjacent contemporaneous juvenile volcanic rocks (or volcaniclastics derived from them). The formation of the sodium carbonates of the Fengcheng Formation may have been related to intense evaporation induced by climate warming, excess alkalinity from bacterial sulfate reduction, and brines with high $Na^+/Ca^{2+}+Mg^{2+}$ ratios due to interaction with intermediate-acidic volcanic rocks (or sediments derived from them) and $CO_2$ derived from magma degassing and the decay of organic matter by both aerobic and anaerobic processes. The decreasing abundance of evaporite minerals in Member 3 is consistent with the shift to a cooler climate during the P1 glaciation of the LPIA during the Early Permian.

**CRediT authorship contribution statement**

All the authors listed have made contributions to this work. Deyu Gong: Writing - Original Draft, Conceptualization, Resources, Project administration, Funding acquisition. Zeyang Liu: Writing - Original Draft; Conceptualization, Writing Review & Editing, Supervision, Funding acquisition. Chuanmin Zhou: Writing - Original Draft, Formal analysis. Emma Ownsworth: Formal analysis, Methodology, Review & Editing. David Selby: Writing - Review & Editing, Supervision. Wenjun He: Writing -

Review & Editing, Formal analysis. Zhijun Qin: Writing - Review & Editing, Formal analysis.

## Declaration of competing interest

The authors declare that they have no known competing financial interests or personal relationships that could have appeared to influence the work reported in this paper.

## Acknowledgements

We gratefully acknowledge the funding of National Natural Science Foundation of China (No. 41802177; 42272188; 42303056) and Petrochina Technology Project (No. 2021DJ0206; 2022DJ0507; 2020D-5008-04). Z.L. acknowledges the funding from Sichuan Natural Science Foundation (23NSFSC5461). We thank Geoff Nowell and Chris Ottley of Durham University for laboratory support.

## Data availability

All data analysed during this study are included in this published article (and its supplementary materials).

**Figure 1**. Location of the Junggar Basin, northwest China (a) that comprises both the Western Uplift, Central Depression and Luliang Uplift tectonic zones (b), and location of the Maye 1 drill core utilized in this study (c). Other core sites discussed in the main text are also shown.

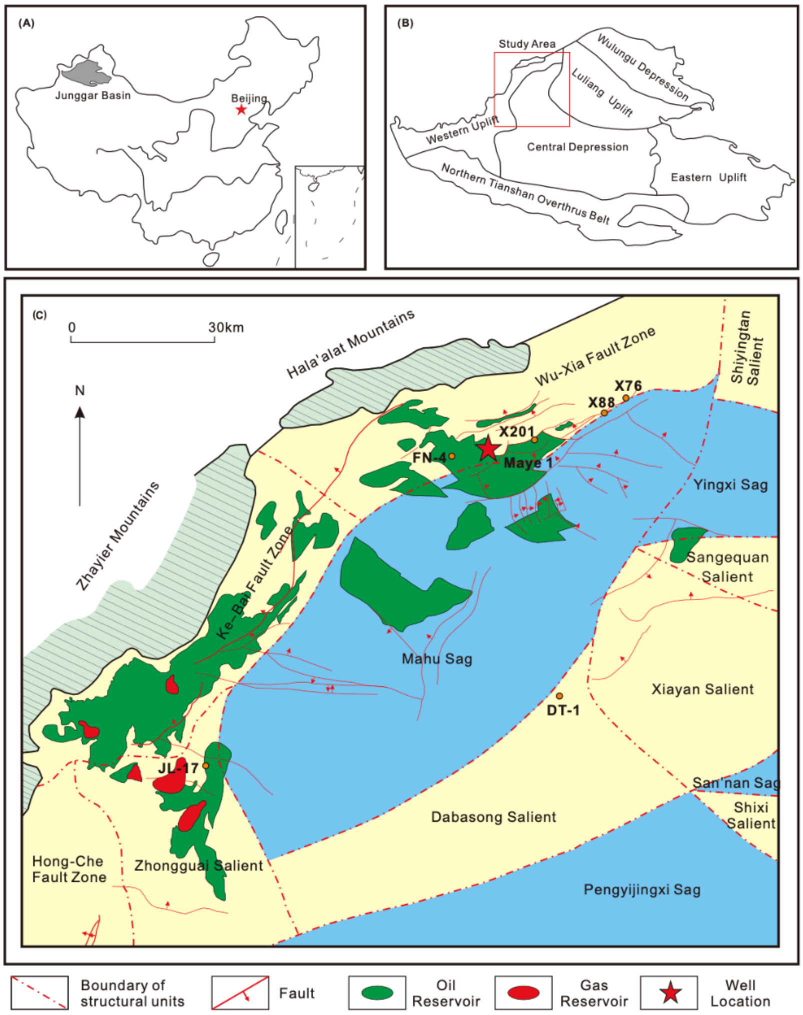

**Figure 2**. Lithological column of the Fengcheng Formation (Members 1, 2 and 3) of the Maye 1 drill core together with total organic carbon (TOC; Table S3), hydrogen index (HI; Table S4), and Re–Os dating (sampled intervals shown by stars) results. Inverse isochron plots were generated using IsoplotR using the $^{187}Re/^{188}Os$ and $^{187}Os/^{188}Os$ data (Table S5; Li and Vermeech, 2021; Vermeech, 2018). Uncertainties are at the 2σ level excluding/including the decay constant uncertainty. Monte Carlo simulations yield identical results to those from the inverse isochron method (uncertainties are presented as analytical only/model uncertainty included). Hexagons represent the equivalent locations of U-Pb ages from Wang et al. 2021 and 2022.

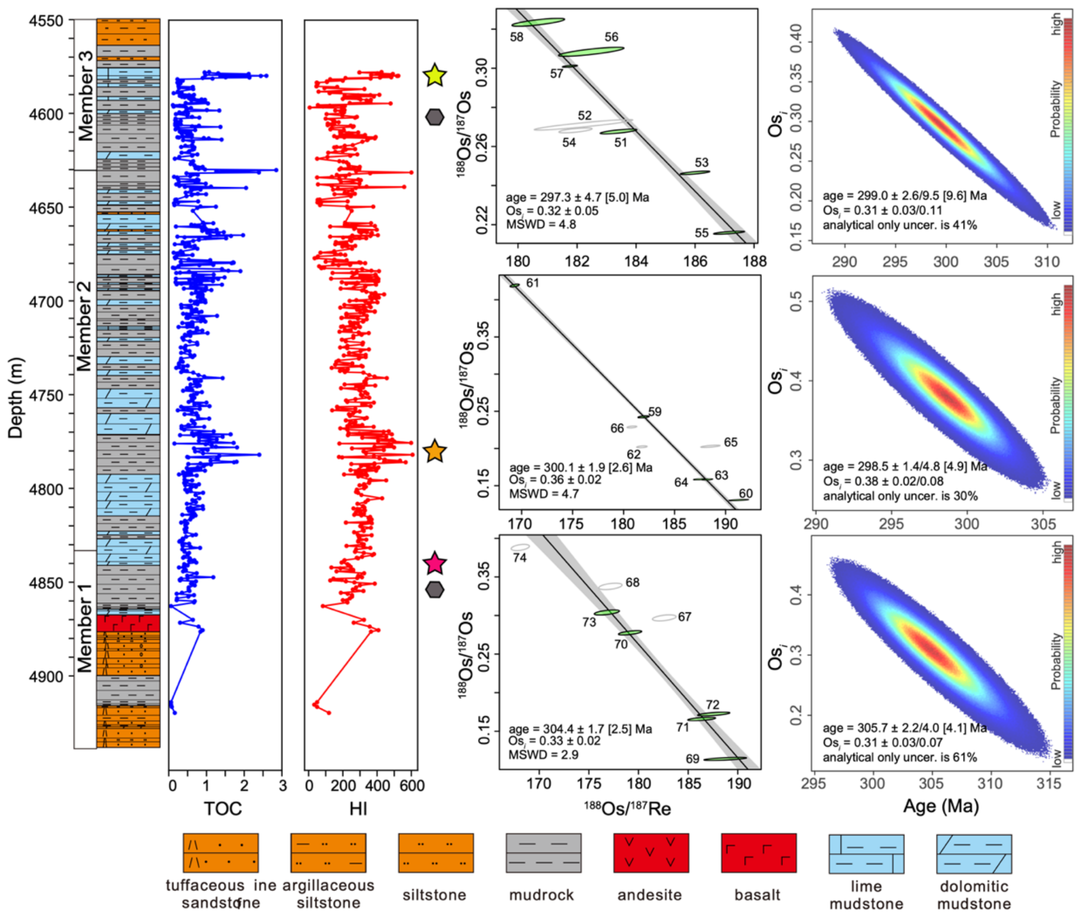

**Figure 3**. Hydrogen-Oxygen index plot showing the kerogen type of the analyzed samples of the Fengcheng Formation (Table S4).

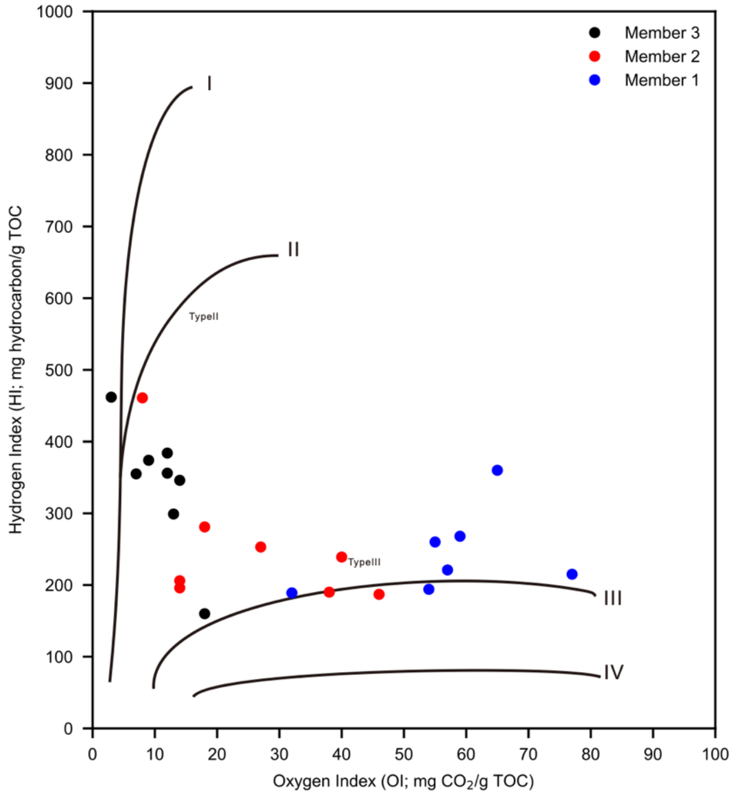

**Figure 4**. Microscopic petrography of macerals through oil immersion. Images A is under blue light. Images B, C and D are under white light. LD: liptinite debit, CD: vitrinite debit, F: fusinite, Cl: clay mineral matrix, Py: pyrite, MiS: microsporinite, V: vitrinite, ID: inertodetrinite, I: Inertinite. See Table S2 for detail.

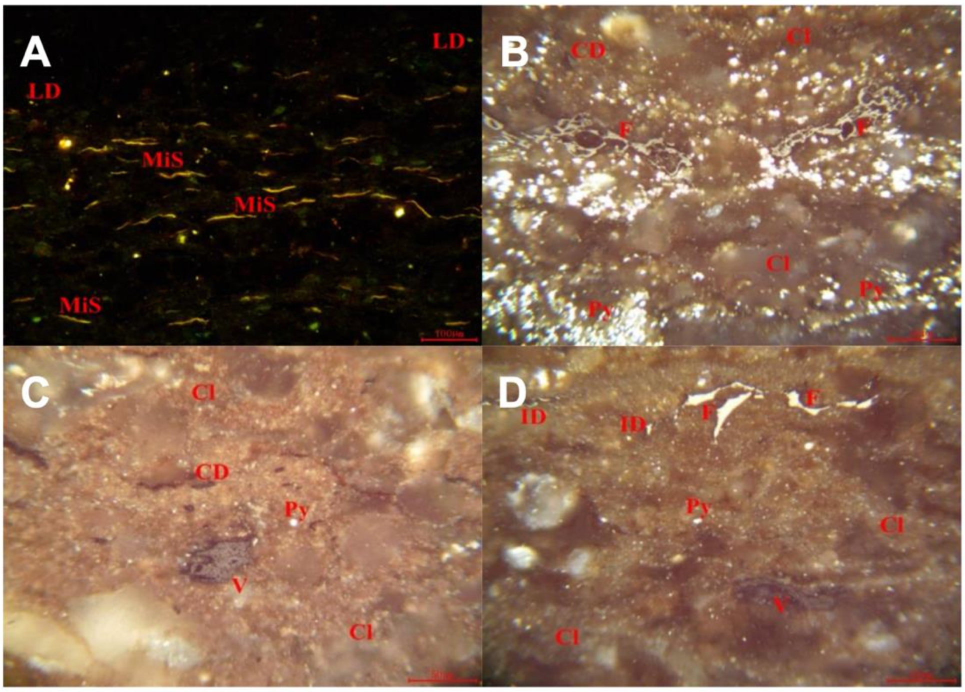

**Figure 5**. Typical evaporite minerals of the Fengcheng Formation in the Mahu Sag. (a) Typical X-ray diffractogram of the bedded evaporite, indicating mineral composition of wegscheuderite, trona, natron, pirssonite, nahcolite and reedmergnerite; (b) A thin bed evaporite observed in the core, composed mainly of trona needles; (c) Thin section photomicrograph (cross-polarized light) of sample from (b), showing columnar trona crystals intercalated with rhombic reedmergnerite crystals; (d) Back-scattered electron image of evaporite from (b), showing columnar trona crystals intercalated with crystals of pirssonite and reedmergnerite; (e) Back-scattered electron image of evaporite from (b), characterized by euhedral–subhedral halite (NaCl) crystals, prismatic nahcolite crystal, and anhedral thenardite ($Na_2SO_4$) crystals, which may occurs as secondary minerals during sample preparation (e.g. Ion milling); (f) Energy dispersive X-ray spectroscopy of natron from(d), with element Au indicating gold coating; (f) Energy dispersive X-ray spectroscopy of pirssonite from (d), with element Au indicating gold coating.

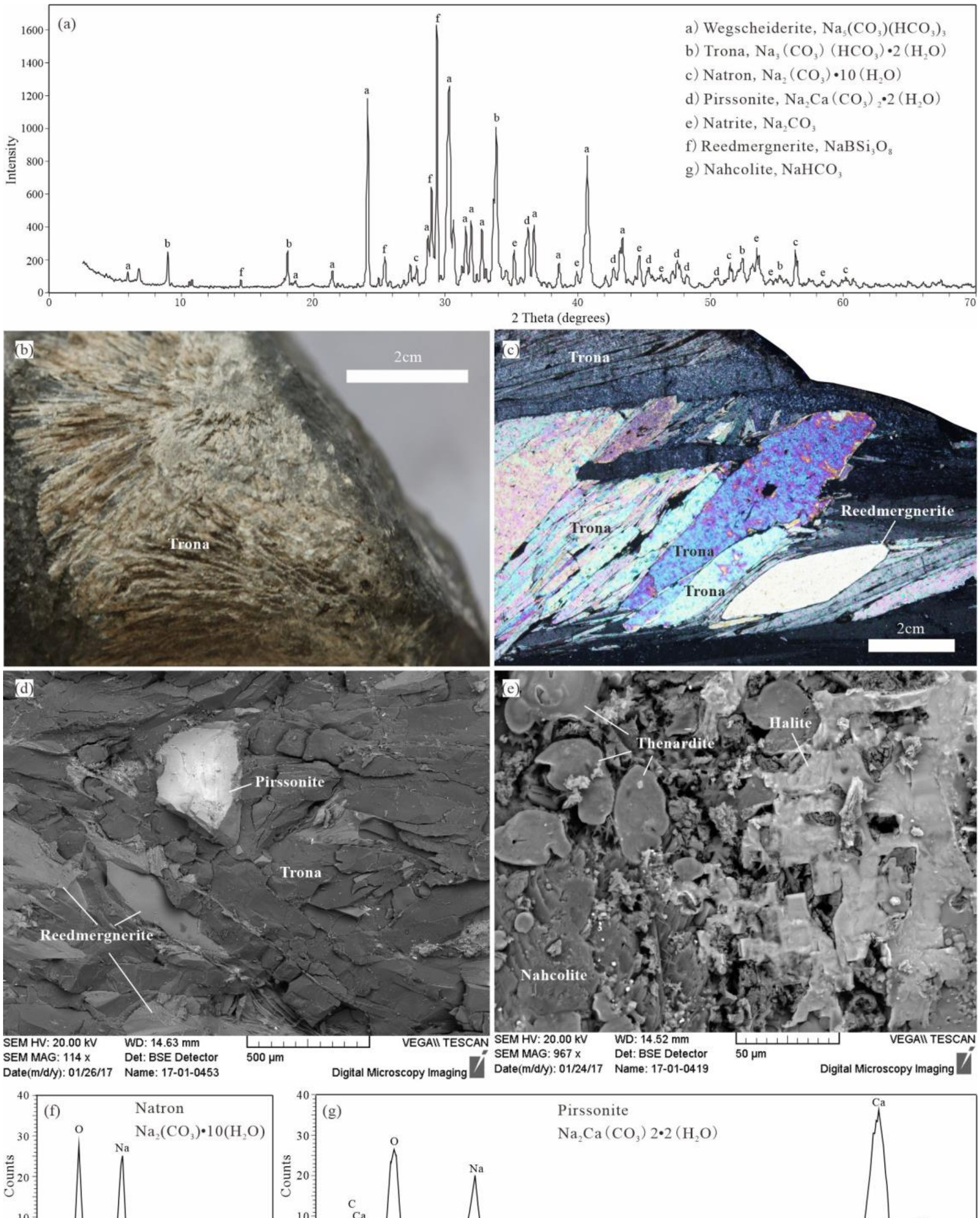
(a)
a) Wegscheiderite, $Na_5(CO_3)(HCO_3)_3$
b) Trona, $Na_3(CO_3)(HCO_3)\cdot 2(H_2O)$
c) Natron, $Na_2(CO_3)\cdot 10(H_2O)$
d) Pirssonite, $Na_2Ca(CO_3)_2\cdot 2(H_2O)$
e) Natrite, $Na_2CO_3$
f) Reedmergnerite, $NaBSi_3O_8$
g) Nahcolite, $NaHCO_3$
Intensity
2 Theta (degrees)
(b)
2cm
Trona
(c)
Trona
Reedmergnerite
2cm
(d)
Pirssonite
Trona
Reedmergnerite
SEM HV: 20.00 kV
WD: 14.63 mm
SEM MAG: 114 x
Det: BSE Detector
Date(m/d/y): 01/26/17
Name: 17-01-0453
500 μm
VEGA\\ TESCAN
Digital Microscopy Imaging
(e)
Thenardite
Halite
Nahcolite
SEM HV: 20.00 kV
WD: 14.52 mm
SEM MAG: 967 x
Det: BSE Detector
Date(m/d/y): 01/24/17
Name: 17-01-0419
50 μm
VEGA\\ TESCAN
Digital Microscopy Imaging
(f)
Natron
$Na_2(CO_3)\cdot 10(H_2O)$
Counts
X-Ray Energy(keV)
(g)
Pirssonite
$Na_2Ca(CO_3)2\cdot 2(H_2O)$
Counts
X-Ray Energy(keV)

**Figure 6**. Age model of the Fengcheng Formation based on different dating methods. Stratigraphic column A) LA-ICP-MS U-Pb detrital zircon from Member 1 and the Fengcheng Formation; B) LA-ICP-MS U-Pb zircon from interbedded tuff beds of Members 1 and 3; C) Re-Os dates from Members 1, 2, and 3 of this study. Glaciation intervals of C3, C4, P1-3 are from Fielding et al. (2008).

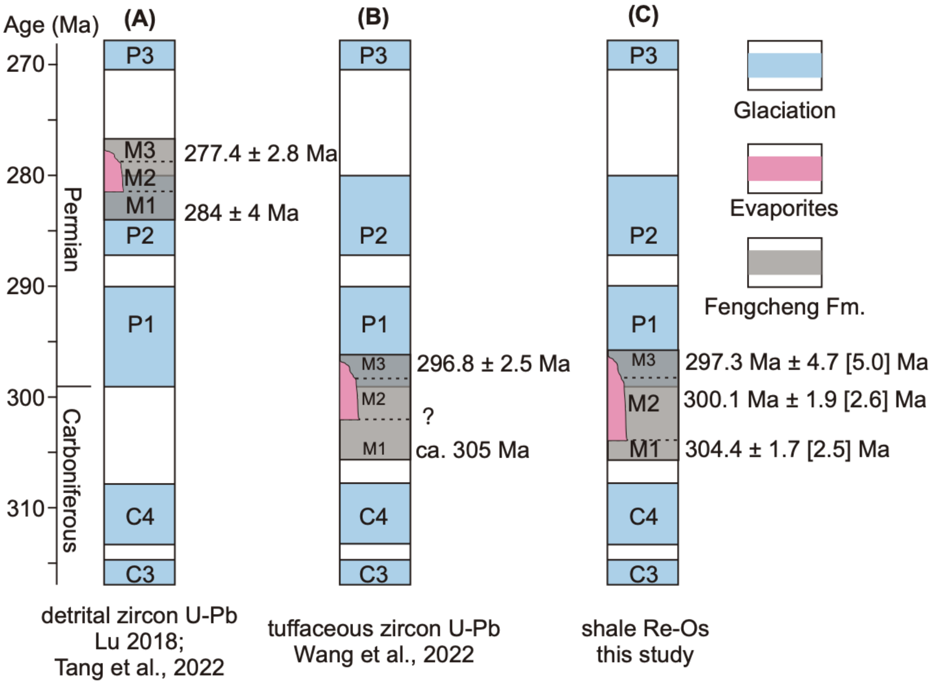

**Figure 7**. Published $^{187}Os/^{188}Os$ ($Os_i$) of the seawater throughout the Carboniferous and Permian (Liu et al., 2020b; Liu et al., 2019; Tripathy et al., 2015; Yano et al., 2022) and for the Fengcheng Formation of this study. Also shown are the paleo-lake values from the Jurassic Da'anzhai Formation (Sichuan Basin, Xu et al., 2017), and average riverine and mantle values (Peucker-Ehrenbrink and Ravizza, 2000). See text for discussion.

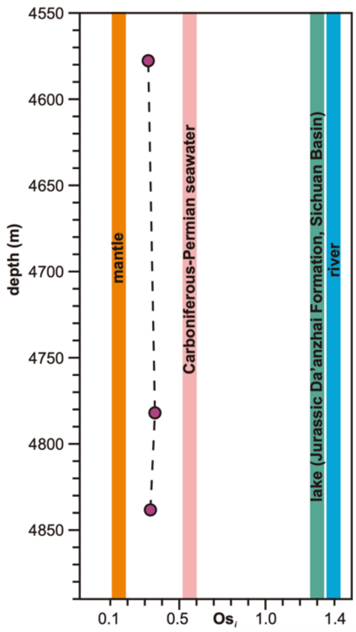

**Table 1. Mole ratio of $Na^+/(Mg^{2+}+Ca^{2+})$ of andesites from the Fengcheng Formation and average andesites.**

| Dataset | Major element (wt. %) | | | | | | | | | Mole ratio of Na/(Mg+Ca) | References |
|---|---|---|---|---|---|---|---|---|---|---|---|
| | $SiO_2$ | $Al_2O_3$ | $Fe_2O_3$ | FeO | MgO | CaO | $Na_2O$ | $K_2O$ | $TiO_2$ | | |
| 1 | 59.500 | 17.20 | 0.00 | 6.10 | 3.42 | 7.03 | 3.68 | 1.60 | 0.70 | 0.56 | Taylor (1968) |
| 2 | 61.68 | 15.84 | 8.52 | / | 3.04 | 3.52 | 4.67 | 1.05 | 1.20 | 1.09 | This study, compiled from Shao et al. (2022) |

## References


Amijaya, H., and Littke, R., 2006, Properties of thermally metamorphosed coal from Tanjung Enim Area, South Sumatra Basin, Indonesia with special reference to the coalification path of macerals: International Journal of Coal Geology, v. 66, no. 4, p. 271–295.

Birck, J.L., Barman, M.R., and Capmas, F., 1997, Re-Os Isotopic Measurements at the Femtomole Level in Natural Samples: Geostandards Newsletter, v. 21, p. 19–27.

Boehrer, B., and Schultze, M., 2008, Stratification of lakes: Reviews of Geophysics, v. 46, no. 2.

Boros, E., and Kolpakova, M., 2018, A review of the defining chemical properties of soda lakes and pans: An assessment on a large geographic scale of Eurasian inland saline surface waters: PLOS ONE 13, doi.org/10.1371/journal.pone.0202205.

Cao, J., Xia, L., Wang, T., Zhi, D., Tang, Y., and Li, W., 2020, An alkaline lake in the Late Paleozoic Ice Age (LPIA): A review and new insights into paleoenvironment and petroleum geology: Earth-Science Reviews, v. 202, p. 103091.

Carroll, A.R., Graham, S.A., Hendrix, M.S., Ying, D., and Zhou, D., 1995, Late Paleozoic tectonic amalgamation of northwestern China: Sedimentary record of the northern Tarim, northwestern Turpan, and southern Junggar Basins: GSA Bulletin, v. 107, no. 5, p. 571–594.

Cohen, A.S., and Waters, F.G., 1996, Separation of osmium from geological materials by solvent extraction for analysis by thermal ionisation mass spectrometry: Analytica Chimica Acta, v. 332, no. 2–3, p. 269–275.

Cumming, V.M., Selby, D., and Lillis, P.G., 2012, Re–Os geochronology of the lacustrine Green River Formation: Insights into direct depositional dating of lacustrine successions, Re–Os systematics and paleocontinental weathering: Earth and Planetary Science Letters, v. 359–360, p. 194–205.

De Cort, G., Bessems, I., Keppens, E., Mees, F., Cumming, B., and Verschuren, D., 2013, Late-Holocene and recent hydroclimatic variability in the central Kenya Rift Valley: The sediment record of hypersaline lakes Bogoria, Nakuru and Elementeita: Palaeogeography, Palaeoclimatology, Palaeoecology, v. 388, p. 69–80.

Dickson, A.J., Cohen, A.S., Coe, A.L., Davies, M., Shcherbinina, E.A., Gavrilov, Y.O., 2015. Evidence for weathering and volcanism during the PETM from Arctic Ocean and Peri-Tethys osmium isotope records. Palaeogeography, Palaeoclimatology, Palaeoecology 438, 300-307.

Du Vivier, A.D.C., Selby, D., Condon, D.J., Takashima, R., and Nishi, H., 2015, Pacific $^{187}Os/^{188}Os$ isotope chemistry and U–Pb geochronology: Synchroneity of global

Os isotope change across OAE 2: Earth and Planetary Science Letters, v. 428, p. 204–216.
Du Vivier, A.D.C., Selby, D., Sageman, B.B., Jarvis, I., Gröcke, D.R., and Voigt, S., 2014, Marine $^{187}Os/^{188}Os$ isotope stratigraphy reveals the interaction of volcanism and ocean circulation during Oceanic Anoxic Event 2: Earth and Planetary Science Letters, v. 389, p. 23–33.
Duarte, C.M., Prairie, Y.T., Montes, C., Cole, J.J., Striegl, R., Melack, J., and Downing, J.A., 2008, $CO_2$ emissions from saline lakes: A global estimate of a surprisingly large flux: Journal of Geophysical Research–Biogeosciences, v. 113, no. G4.
Duckworth, A.W., Grant, W.D., Jones, B.E., and van Steenbergen, R., 1996, Phylogenetic diversity of soda lake alkaliphiles: FEMS Microbiology Ecology, v. 19, no. 3. p. 181–191.
Earman, S., Phillips, F.M., and McPherson, B.J.O.L., 2005, The role of “excess” $CO_2$ in the formation of trona deposits: Applied Geochemistry, v. 20, no. 12, p. 2217–2232.
Eugester, H.P., and Hardie, L., 1978, Saline lakes, Lakes: Chemistry, Geology and Physics. Springer-Verlag New York, pp. 237–293.
Eugster, H.P., 1966, Sodium carbonate-bicarbonate minerals as indicators of $PCO_2$: Journal of Geophysical Research (1896-1977), v. 71, p. 3369–3377.
Feng, J., Dai, J., Li, X., and Luo, P., 2018, Soft collision and polyphasic tectonic evolution of Wuxia foreland thrust belt: Evidence from geochemistry and geophysics at the northwestern margin of the Junggar Basin: Journal of Geodynamics, v. 118, p. 32–48.
Fielding, C.R., Frank, T.D., Birgenheier, L.P., 2023. A revised, late Palaeozoic glacial time-space framework for eastern Australia, and comparisons with other regions and events. Earth-Science Reviews 236, 104263.
Gao, Y., Huang, H., Tao, H., Carroll, A.R., Qin, J., Chen, J., Yuan, X., Wang, C., 2020. Paleoenvironmental setting, mechanism and consequence of massive organic carbon burial in the Permian Junggar Basin, NW China. Journal of Asian Earth Sciences 194, 104222.
Gong, D., Liu, Z., He, W., Zhou, C., Qin, Z., Wei, Y., Yang, C., 2024. Multiple enrichment mechanisms of organic matter in the Fengcheng Formation of Mahu Sag, Junggar Basin, NW China. Petroleum Exploration and Development 51, 292-306.
Grant, W.D., Mwatha, W.E., and Jones, B.E., 1990, Alkaliphiles: Ecology, diversity and applications: FEMS Microbiology Letters, v. 75, no. 2–3, p. 255–269.
Helfer, F., Lemckert, C., and Zhang, H., 2012, Impacts of climate change on temperature and evaporation from a large reservoir in Australia: Journal of Hydrology, v. 475, p. 365–378.
Jagniecki, E.A., Lowenstein, T.K., Jenkins, D.M., and Demicco, R.V., 2015, Eocene atmospheric $CO_2$ from the nahcolite proxy: Geology, v. 43, no. 12, p. 1075–1078.

Jones, B.F., Eugster, H.P., and Rettig, S.L., 1977, Hydrochemistry of the Lake Magadi basin, Kenya: Geochimica et Cosmochimica Acta, v. 41, no. 1, p. 53–72.

Kato, Y., Fujinaga, K., and Suzuki, K., 2011, Marine Os isotopic fluctuations in the early Eocene greenhouse interval as recorded by metalliferous umbers from a Tertiary ophiolite in Japan: Gondwana Research, v. 20, no. 2–3, p. 594–607.

Kemp, D.B., Selby, D., and Izumi, K., 2020, Direct coupling between carbon release and weathering during the Toarcian oceanic anoxic event: Geology, v. 48, no. 10, p. 976–980.

Kusakabe, M., Ohba, T., Issa, Yoshida, Y., Satake, H., Ohizumi, T., Evans, W.C., Tanyileke, G., and Kling, G.W., 2008, Evolution of $CO_2$ in Lakes Monoun and Nyos, Cameroon, before and during controlled degassing: Geochemical Journal, v. 42, no. 1, p. 93–118.

Li, D., He, D., and Fan, C., 2015, Geochronology and Sr–Nd–Hf isotopic composition of the granites, enclaves, and dikes in the Karamay area, NW China: Insights into late Carboniferous crustal growth of West Junggar: Geoscience Frontiers, v. 6, no. 2, p. 153–173.

Li, Y., and Vermeesch, P., 2021, Inverse isochron regression for Re–Os, K–Ca and other chronometers: Geochronology, v. 3, p. 415–420. doi.org/10.5194/gchron-2021-7.

Li, Y., Zhang, S., Hobbs, R., Caiado, C., Sproson, A.D., Selby, D., and Rooney, A.D., 2019, Monte Carlo sampling for error propagation in linear regression and applications in isochron geochronology: Science Bulletin, v. 64, p. 189–197.

Liu, Z., and Selby, D., 2021, Deep-water osmium-isotope record of the Permian–Triassic interval from Niushan, China reveals potential delayed volcanic signal post the mass extinction: Global and Planetary Change, v. 200, p. 103473.

Liu, Z., Selby, D., Hackley, P.C., and Over, D.J., 2020a, Evidence of wildfires and elevated atmospheric oxygen at the Frasnian–Famennian boundary in New York (USA): Implications for the Late Devonian mass extinction: GSA Bulletin, v. 132, no. 9–10, p. 2043–2054.

Liu, Z., Selby, D., Zhang, H., and Shen, S., 2020b, Evidence for volcanism and weathering during the Permian-Triassic mass extinction from Meishan (South China) osmium isotope record: Palaeogeography: Palaeoclimatology, Palaeoecology, v. 553, p. 109790.

Liu, Z., Selby, D., Zhang, H., Zheng, Q., Shen, S., Sageman, B.B., Grasby, S.E., and Beauchamp, B., 2019, Osmium-isotope evidence for volcanism across the Wuchiapingian–Changhsingian boundary interval: Chemical Geology, v. 529, p. 119313.

Lowenstein, T.K., Jagniecki, E.A., Carroll, A.R., Smith, M.E., Renaut, R.W., and Owen, R.B., 2017, The Green River salt mystery: What was the source of the hyperalkaline lake waters?: Earth-Science Reviews, v. 173, p. 295–306.

Lu, Y., 2018, Permian chronostratigraphic framework and sedimentary filling evolution in Mahu-Shawan and adjacent area, Junggar Basin [M.S. thesis]: Wuhan, China, China University of Geosciences.

Lúcio, T., Souza Neto, J.A., and Selby, D., 2020, Late Barremian / Early Aptian Re–Os age of the Ipubi Formation black shales: Stratigraphic and paleoenvironmental implications for Araripe Basin, northeastern Brazil: Journal of South American Earth Sciences, v. 102, p. 102699.

Milton, C., and Fahey, J.J., 1960, Classification and association of the carbonate minerals of the Green River Formation: American Journal of Science, v. 258, p. 242–246.

Montañez, I.P., and Poulsen, C.J., 2013, The Late Paleozoic Ice Age: An Evolving Paradigm: Annual Review of Earth and Planetary Sciences, v. 41, p. 629–656.

Muyzer, G., and Stams, A.J.M., 2008, The ecology and biotechnology of sulphate-reducing bacteria: Nature Reviews Microbiology, v. 6, p. 441–454.

Percival, L.M.E., Cohen, A.S., Davies, M.K., Dickson, A.J., Hesselbo, S.P., Jenkyns, H.C., Leng, M.J., Mather, T.A., Storm, M.S., and Xu, W., 2016, Osmium isotope evidence for two pulses of increased continental weathering linked to Early Jurassic volcanism and climate change: Geology, v. 44, no. 9, p. 759–762.

Peucker-Ehrenbrink, and B., Ravizza, G., 2000, The marine osmium isotope record: Terra Nova, v. 12, no. 5, p. 205–219.

Pietras, J.T., Dennett, A., Selby, D., and Birdwell, J.E., 2022, The role of organic matter diversity on the Re-Os systematics of organic-rich sedimentary units: Insights into the controls of isochron age determinations from the lacustrine Green River Formation: Chemical Geology, v. 604, p. 120939.

Poirier, A., and Hillaire-Marcel, C., 2011, Improved Os-isotope stratigraphy of the Arctic Ocean: Geophysical Research Letters, v. 38.

Schmitz, M.D., 2020, Appendix 2 - Radioisotopic ages used in GTS2020, in: Gradstein, F.M., Ogg, J.G., Schmitz, M.D., Ogg, G.M. (Eds.), Geologic Time Scale 2020. Elsevier, pp. 1285–1349.

Selby, D., and Creaser, R.A., 2003, Re–Os geochronology of organic rich sediments: an evaluation of organic matter analysis methods: Chemical Geology, v. 200, no. 3–4, p. 225–240.

Selby, D., Creaser, R.A., and Fowler, M.G., 2007, Re–Os elemental and isotopic systematics in crude oils: Geochimica et Cosmochimica Acta, v. 71, no. 2, p. 378–386.

Şengör, A.M.C., Natal'in, B.A., and Burtman, V.S., 1993, Evolution of the Altaid tectonic collage and Palaeozoic crustal growth in Eurasia: Nature, v. 364, p. 299–307.

Shao, L.F., Yu, F.S., Wang D.D., Li C., 2022. Geochronology, geochemistry, and tectonic significance of Carboniferous Andesite in the Zhongguai Uplift, Northwestern Margin of the Junggar Basin. Geoscience 36( 3), 812-823. (in Chinese with English abstract).

Smoliar, M.I., Walker, R.J., and Morgan, J.W., 1996, Re-Os ages of group IIA, IIIA, IVA, and IVB iron meteorites: Science, v. 271, no. 5252, p. 1099–1102.

Sproson, A.D., Pogge von Strandmann, P.A.E., Selby, D., Jarochowska, E., Frýda, J., Hladil, J., Loydell, D.K., Slavík, L., Calner, M., Maier, G., Munnecke, A., Lenton, T.M., 2022. Osmium and lithium isotope evidence for weathering feedbacks linked to orbitally paced organic carbon burial and Silurian glaciations. Earth and Planetary Science Letters 577, 117260.

Svensen, H., Planke, S., Polozov, A.G., Schmidbauer, N., Corfu, F., Podladchikov, Y.Y., and Jamtveit, B., 2009, Siberian gas venting and the end-Permian environmental crisis: Earth and Planetary Science Letters, v. 277, no. 3–4, p. 490–500.

Tang, G.J., Wyman, D.A., Wang, Q., Li, J., Li, Z.X., Zhao, Z.H., and Sun, W.D., 2012, Asthenosphere–lithosphere interaction triggered by a slab window during ridge subduction: Trace element and Sr–Nd–Hf–Os isotopic evidence from Late Carboniferous tholeiites in the western Junggar area (NW China): Earth and Planetary Science Letters, v. 329–330, p. 84–96.

Tang, W., Zhang, Y., Pe-Piper, G., Piper, D.J.W., Guo, Z., and Li, W., 2021, Permian rifting processes in the NW Junggar Basin, China: Implications for the post-accretionary successor basins: Gondwana Research, v. 98, p. 107–124.

Tang, J., He, D., Li, D., Ma, D., 2015. Large-scale thrusting at the northern Junggar Basin since Cretaceous and its implications for the rejuvenation of the Central Asian Orogenic Belt. Geoscience Frontiers 6, 227-246.

Taylor, G., Teichmüller, M., Davis, A., Diessel, C., Littke, R., and Robert, P., 1998, Organic Petrology.

Taylor, S.R., 1968. Geochemistry of Andesites, in: Ahrens, L.H. (Ed.), Origin and Distribution of the Elements. Pergamon, pp. 559–583.

Them, T.R., Gill, B.C., Selby, D., Gröcke, D.R., Friedman, R.M., and Owens, J.D., 2017, Evidence for rapid weathering response to climatic warming during the Toarcian Oceanic Anoxic Event: Scientific Reports, v. 7, p. 5003.

Timms, B.V., 2022. Salt Lakes, in: Mehner, T., Tockner, K. (Eds.), Encyclopedia of Inland Waters (Second Edition). Elsevier, Oxford, pp. 141-156.

Tosca, N.J., Tutolo, B.M., 2023. How to Make an Alkaline Lake: Fifty Years of Chemical Divides. Elements 19, 15-21.

Tripathy, G.R., Hannah, J.L., Stein, H.J., Geboy, N.J., and Ruppert, L.F., 2015, Radiometric dating of marine-influenced coal using Re–Os geochronology: Earth and Planetary Science Letters, v. 432, p. 13–23.

Vermeesch, P., 2018, IsoplotR: A free and open toolbox for geochronology: Geoscience Frontiers, v. 9, no. 5, p. 1479–1493.

Wang, T., Cao, J., Carroll, A.R., Zhi, D., Tang, Y., Wang, X., and Li, Y., 2021, Oldest preserved sodium carbonate evaporite: Late Paleozoic Fengcheng Formation, Junggar Basin, NW China: GSA Bulletin, v. 133, no. 7–8, p. 1465–1482.

Wang, T., Cao, J., Xia, L., Zhi, D., Tang, Y., and He, W., 2022, Revised age of the Fengcheng Formation, Junggar Basin, China: Global implications for the late Paleozoic ice age: Global and Planetary Change, v. 208, p. 103725.

Wang, X., Gao, J., Zhong, L., He, W., Jin, Z., Zhu, R., Liang, X., Liu, K., Zhang, W., 2022, The Volcanic Impacts on the Formation of Organic-Rich Shales From the Freshwater to Saline Lakes: Cases Study in the Ordos and the Junggar Basins: Frontiers in Earth Science, v. 10.

Warren, J.K., 2010, Evaporites through time: Tectonic, climatic and eustatic controls in marine and nonmarine deposits: Earth-Science Reviews, v. 98, no. 3–4, p. 217–268.

Whittig, L., and Janitzky, P., 1963, Mechanisms of formation of sodium carbonate in soils: I. Manifestations of biological conversions: Journal of Soil Science, v. 14, p. 322–333.

Xia, L., Cao, J., Hu, W., Stüeken, E.E., Wang, X., Yao, S., Zhi, D., Tang, Y., Xiang, B., He, W., 2023, Effects on global warming by microbial methanogenesis in alkaline lakes during the Late Paleozoic Ice Age (LPIA): Geology, v. 51, p. 935-940.

Xu, W., Ruhl, M., Jenkyns, H.C., Hesselbo, S.P., Riding, James.B., Selby, D., Naafs, B.D.A., Weijers, J.W.H., Pancost, Richard.D., Tegelaar, Erik.W., and Idiz, E.F., 2017, Carbon sequestration in an expanded lake system during the Toarcian oceanic anoxic event: Nature Geoscience, v. 10, p. 129–134.

Yang, F., Li, J., Lu, S., Bian, B., Liu, H., Wei, Y., Qi, X., Yang, H., 2023. Carboniferous to Early Permian tectono-sedimentary evolution in the western Junggar Basin, NW China: implication for the evolution of Junggar Ocean. Frontiers in Earth Science 11.

Yang, J.H., Yi, C.L., Du, Y.S., Zheang, Z.H., Yan, J.X., 2014. Geochemical significance of the Paleogene soda-deposits bearing strata in Biyang Depression, Henan Province. Sci. China: Earth Sci. 44, 2172–2181. https://doi.org/10.1360/zd-2014-44-10-2172.

Yang, Y.-T., Song, C.-C., He, S., 2015. Jurassic tectonostratigraphic evolution of the Junggar basin, NW China: A record of Mesozoic intraplate deformation in Central Asia. Tectonics 34, 86-115.

Yano, M., Yasukawa, K., Nozaki, T., Fujinaga, K., Ohta, J., Nakamura, K., and Kato, Y., 2022, Marine osmium isotopic composition reconstructed from the early Permian umber deposit in the Japanese accretionary complex: Journal of Asian Earth Sciences, v. 241, p. 105480.

Zhang, Y., Qi, X., Cheng, X., and Luo Z., 2007, Approach to sedimentary environment of Late Carboniferous-Permian in Junggar basin: Xinjiang Petroleum Geology, v. 28, no. 6, p. 673–675 (in Chinese with English abstract).